RSC Applied Polymers

ROYAL SOCIETY OF CHEMISTRY

PAPER

View Article Online
View Journal | View Issue

Cite this: *RSC Appl. Polym.*, 2025, **3**, 1230

Printable fluorinated poly(ionic liquid)-ionic liquid composite membranes for fluorinated gas separation†

Randinu Pulukkody,[a] Chia-Min Hsieh,‡[a] Abby N. Harders,‡[b] Yuniva Mendoza-Apodaca,[b] Mark B. Shiflett[b] and Emily B. Pentzer *[a,c]

Received 20th January 2025,
Accepted 8th June 2025

DOI: 10.1039/d5lp00014a

rsc.li/rscapplpolym

Membrane technology offers a compelling approach for separating hydrofluorocarbon (HFC) refrigerant mixtures, primarily due to lower energy demands and lower capital investment compared to traditional separation techniques. Herein, we report the development of fluorinated poly(ionic liquid)-ionic liquid composite membranes, combining the advantageous properties of both polymers and ionic liquids (ILs), for HFC gas separation. Two vinyl imidazolium-based fluorinated ionic liquid (FIL) monomers were synthesized, along with two FILs containing complementary cations and anions, which were incorporated as "free" liquid. Free-standing, IL-containing membranes were prepared by photopolymerization of the FIL-based monomer and a crosslinker in the presence of free IL. As a complementary study, membranes were also prepared from a methacrylate-based non-fluorinated imidazolium IL monomer with 1-hexyl-3-methylimidazolium bis(trifluoromethylsulfonyl)imide ($[C_6C_1im][Tf_2N]$) as free IL. The extent of crosslinking and the relationship between membrane composition and thermal properties are reported. Pure-gas permeability of commonly used HFC gases, specifically HFC-32 (difluoromethane) and HFC-125 (pentafluoroethane), were evaluated. For all membranes, HFC-32 had higher permeability than HFC-125. Finally, we demonstrate the use of digital light processing (DLP) additive manufacturing to print the membranes, presenting a promising avenue for the rapid fabrication of bespoke membranes for difficult separations.

1. Introduction

Ionic liquids (ILs), characterized by their high chemical and thermal stability, non-volatility, and tunable structures, have been extensively explored for gas uptake and separation applications.[1–4] A notable emerging application of ILs is in the absorption and separation of refrigerant hydrofluorocarbon (HFC) gases. Currently, most refrigerant gas mixtures in global circulation contain HFCs with high global warming potentials (GWPs) and exhibit azeotropic behavior, making the separation and reclamation of the gas components challenging.[5] Consequently, the use of tailored ILs as solvents for the selective solubilization of HFC gases has received significant interest. For instance, Shiflett and coworkers conducted comprehensive studies on the application of commercially available ILs for the absorption of HFC-32 and HFC-125, constituents of the refrigerant R-410A.[6,7] The authors identified the selective solubility of HFC-32 in fluorine-containing ILs and the preferential solubility of HFC-125 in ILs composed of cations bearing long alkyl chains.[6,7] Despite the promising results of HFC gas uptake using ILs, the large volumes of circulating solvents required for practical applications pose a significant challenge due to the high cost and viscosity of ILs, limiting their use as bulk liquids. To address these issues, recent advancements have focused on developing polymer membranes for gas uptake and separation applications.

Fluoropolymer membranes, particularly those derived from copolymers of perfluoro(butenyl vinyl ether) (PBVE) and perfluoro(2,2-dimethyl-1,3-dioxole) (PDD), have been studied for their application in HFC gas separation.[8,9] These membranes possess high permeability and selectivity for HFC gases, which has been attributed to higher fractional free volume due to lower packing of the highly fluorinated polymer chains.[8,9] For instance, Harders *et al.* reported the use of 5% PBVE–95% PDD copolymer membranes to separate R-410A components (*i.e.*, HFC-32 and HFC-125).[8] Their findings revealed selective

[a]*Department of Chemistry, Texas A&M University, College Station, TX 77843, USA. E-mail: emilypentzer@tamu.edu*
[b]*Department of Chemical & Petroleum Engineering, University of Kansas, Lawrence, KS, 66045, USA*
[c]*Department of Materials Science and Engineering, Texas A&M University, College Station, TX, 77843, USA*

†Electronic supplementary information (ESI) available. See DOI: https://doi.org/10.1039/d5lp00014a

‡These authors contributed equally to this work.

permeation HFC-32, achieving permeabilities as high as 360 Barrer for HFC-32 but only 30 Barrer for HFC-125, thus a selectivity of ~14. Despite their advantageous properties, fluoropolymer membranes also present significant challenges. The synthesis of PBVE and PDD monomers is notably complex and costly, involving multiple steps and expensive raw materials.[10] This complexity limit the widespread adoption of these membranes for gas separation applications and limit the evaluation of structure–performance relationships.

A novel class of membranes that has emerged with promising applications in gas separation is composites of ILs and polymers,[11–13] integrating the unique physicochemical properties of ILs with the mechanical properties of polymers. Compared to polymers alone, permeability and selectivity can be enhanced by incorporating ILs into the polymer membranes. Compared to bulk ILs, IL/polymer membranes offer the advantage of a higher surface area-to-volume ratio, leading to more efficient separation processes, as well as reducing the quantity of IL required, lowering costs and minimizing potential environmental impacts.[11] The confinement of ILs within a polymer matrix also mitigates issues related to mass transfer in bulk ILs. Early work on IL/polymer membranes focused on supported IL membranes (SILMs), where ILs were immobilized within a porous polymeric support.[14] SILMs operate *via* a solubility–diffusivity mechanism, whereby gas molecules dissolve in the IL and subsequently diffuse through the membrane[14–16] and they have been extensively utilized for carbon capture.[12,14,17,18] For example, Santos *et al.* immobilized imidazolium acetate ILs within a polyvinylidene fluoride support for the selective separation of CO_2 from N_2.[19] They observed CO_2 permeance values ranging from 852 to 2114 Barrers, with permeability increasing as the temperature rose. The selectivity between CO_2 and N_2 ranged from 26 to 39, decreasing at higher temperatures. The permeability values significantly exceeded those reported in other studies using polymeric membranes,[20–22] where CO_2 permeability was typically <1000 Barrers. Despite their promising advantages for gas separation, the stability of SILMs remains a significant challenge for large-scale and long-term applications, as IL leakage can occur during continuous operation.[23] An ideal membrane for the separation of gases, including HFCs, would have high permeability, minimizing the membrane area required to process a specific volume of gas, and high selectivity, enhancing the purity of the separated gas.

To address the limitations of SILMs, considerable focus has shifted towards the development of poly(IL)-IL composite membranes. These membranes are prepared by polymerizing IL-based monomers in the presence of "free" IL, thereby producing a polymer (polyIL) matrix loaded with the IL. This approach maintains the tunable ionic properties and high thermal stability of ILs while enhancing mechanical strength and processability. To date, composite poly(IL)-IL membranes have mainly been utilized for CO_2 capture. For instance, Bara and coworkers synthesized anionic poly(IL)-IL membranes using IL monomers with highly delocalized anions ($-SO_2-N^(-)-SO_2-CF_3$ and $-SO_2-N^(-)-SO_2-C_7H_7$) and mobile imidazolium countercations ($[C_2C_1im]^+$).[24] These monomers were photopolymerized with a crosslinker and varying amounts of free IL, with the free IL having the same cation structure as the monomer. Their findings revealed a significant increase in CO_2 permeability from 7.6 Barrers to 20.4 Barrers when the pendant group was changed from $-CF_3$ to $-C_7H_7$. This improvement was attributed to enhanced gas diffusivity resulting from increased polymer chain flexibility, as confirmed through wide-angle X-ray scattering (WAXS). Given the promising results of gas separation using poly(IL)-IL composite membranes, there is a unique opportunity to develop poly(IL)-IL membranes for refrigerant HFC gas separation. Building on previous literature highlighting the influence of fluorination in ILs on HFC gas uptake,[3,4,7] the development of novel fluorinated poly(IL)-IL composite membranes is of particular interest.

Herein, we report the synthesis of fluorinated poly(IL)-IL composite membranes and the effects of composition on the physical properties and performance in fluorinated gas separation. Two poly(IL)s are prepared which bear immobilized fluorinated imidazolium cations and mobile fluorinated anions; a non-fluorinated membrane was prepared for comparison. As shown in Fig. 1, the two vinyl-imidazolium-based fluorinated monomers M-1 and M-2 bear pendant fluorinated alkyl chains with M-1 bearing a bistriflimide (Tf_2N) anion and M-2 bearing a (2,4-difluorophenyl) ((trifluoromethyl)sulfonyl) amide anion; for each monomer, a complementary "free" IL was used, which bears a similar imidazolium cation and anion (FIL-1 and FIL-2). For comparison, a methacrylate-based IL monomer, previously documented for applications in CO_2 capture, single ion conductors, and polymer antibacterial agents, was used,[25–28] along with the commercially available 1-hexyl-3-methyl imidazolium bistriflimide ($[C_6C_1im][Tf_2N]$) (termed FIL-3 herein). For each system, poly(ethylene glycol) diacrylate (PEGDA) was used as the cross-linker to enhance mechanical stability of the resulting membrane. After membrane preparation and characterization of the thermal properties, gas separation tests using HFC-32 and HFC-125 were performed. All evaluated membranes displayed higher permeability of HFC-32 than HFC-125. Finally, we demonstrate that the additive manufacturing technique of digital light processing (DLP) can be used to print the poly(IL)-IL composites, thereby providing a practical and cost-effective method for the production of membranes with bespoke size and shape.

2. Experimental section

Materials

All chemicals were purchased from commercial sources and used directly as received, unless otherwise stated. *N*-Methylimidazole (99%), 1*H*,1*H*,2*H*,2*H*-perfluorooctyl iodide (97%), 1*H*,1*H*,2*H*,2*H*-perfluorodecyl iodide (96%), 2,2-dimethoxy-2-phenylacetophenone (DMPA) (99%) were purchased from Fisher Scientific. Lithium bis(trifluoromethanesulfonyl)imide (99.9%), sodium metal (in mineral oil, 99.9%),

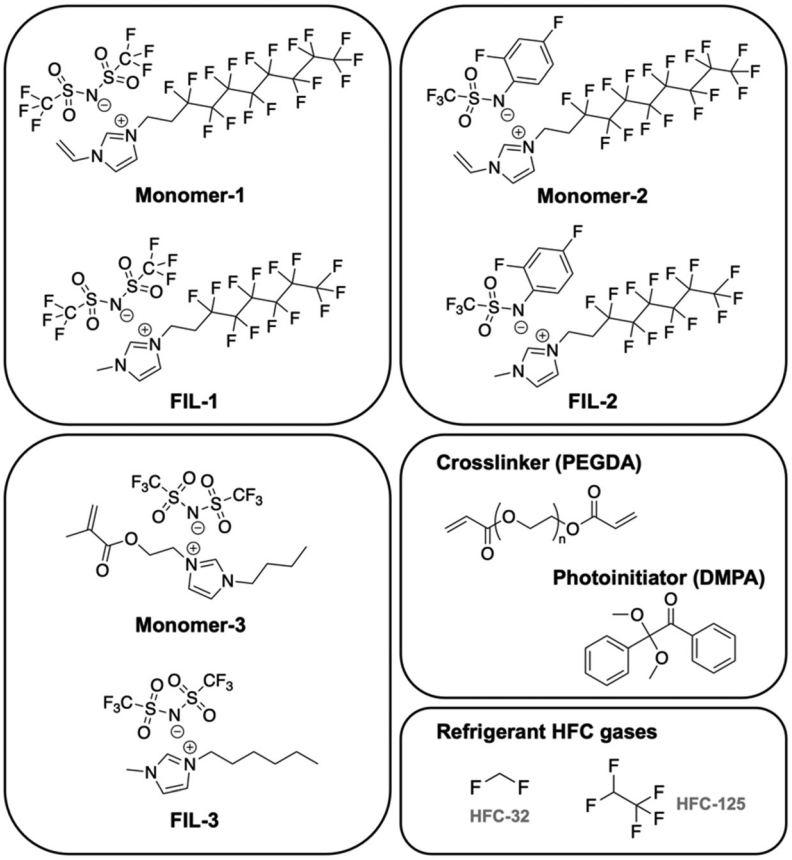

Fig. 1 Structures of monomers, free ILs, crosslinker, and photoinitiator used for membrane preparation, as well as structures of HFC-32 and HFC-125 used for gas permeability measurements.

2,4-difluoroaniline (99%), 2-bromoethanol (95%), methacryloyl chloride (97%), triethylamine (99%), 1-vinylimidazole (99%), polyethylene glycol diacrylate (PEGDA) (M_n = 250), PEGDA (M_n = 575), and methanol (99.8%) were purchased from Sigma Aldrich. 1-Hexyl-3-methyl imidazolium bistriflimide was purchased from Iolitech.

Characterization

^{1}H, ^{13}C, and ^{19}F nuclear magnetic resonance (NMR) spectroscopy was carried out using a Bruker Avance NEO 400 MHz NMR spectrometer using $(CD_3)_2SO$ (DMSO-d_6) as the solvent, with non-deuterated DMSO as a reference peak. Fourier Transform Infrared Spectroscopy (FTIR) data was collected using a JASCO FT/IR-4600 with a ZnSe/diamond prism with 32 scans in ATR mode. Thermogravimetric analysis (TGA) was recorded on a TA Instruments TGA 5500 under N_2 gas. Each sample was heated to 100 °C, equilibrated for 2 min, then ramped to 650 °C at 10 °C min^{-1}. Differential scanning calorimetry (DSC) was carried out on a TA instruments DSC 2500 using hermetically sealed aluminum pans. The samples were first cooled to −80 °C at 10 °C min^{-1}, equilibrated for 1 min, then ramped at 10 °C min^{-1} to a temperature ~50 °C lower than the 5% mass loss temperature determined from TGA. Three cooling-heating cycles were collected for each sample (second cycle is reported).

The 3D printing process was executed using a commercial Flashforge Hunter DLP 3D printer, equipped with a 405 nm projector. The structures were sliced using FlashDLPrint, the CAD software provided by Flashforge. Each structure was composed of 19 printed layers, each with a height of 100 μm, resulting in an overall object height of 1.9 mm. The light intensity was set at 200%, and the exposure time was progressively reduced from 300 s to 60 s over 15 decremental layers to effectively control exposure. After printing, the object was detached from the build platform using a metal spatula and residual liquid resin was removed from the surface with a Kimwipe. All printed structures underwent post-curing using a 365 nm UV flashlight, with 30 s of exposure on each face, totaling 60 s. The resin formulation was the same as that used for membrane preparation by casting, with the exception that the photoinitiator was replaced with phenylbis(2,4,6-trimethylbenzoyl)phosphine oxide (BAPO) to align with the UV light specifications of the printer. Compression test was achieved using a DMA 850 instrument using a compression clamp. Cylindrical samples were compressed from 0 to 15% strain at a rate of 0.25 mm min^{-1}. For characterization by SEM, a conductive carbon double-sided tape was affixed to a stub (Ø 12.7 mm

× 8 mm pin height) serving as the sample substrate and the printed sample was placed onto this, followed by a 10 nm Au coating applied *via* sputter coating using the Cressington 108 Sputter Coater; SEM characterization was conducted using a Tescan Vega.

Gas permeation through polymeric membranes is explained by the solution–diffusion model, where the permeability (P) is a function of both diffusivity and solubility. Permeability is a metric of membrane productivity and describes the flux of a penetrant through a membrane under a pressure gradient. In this research, a constant-volume, pressure-rise apparatus was utilized to determine single-gas permeability of both HFC-32 and HFC-125. Within this instrument, a membrane film of known thickness and area is secured into the static membrane apparatus to separate the upstream volume from the downstream volume. The upstream side of the membrane is pressurized with a pure-component gas and maintained at a constant pressure throughout the experiment. The increase in downstream pressure is measured as a function of time. The permeability of a single component gas can be calculated with the following equation:

$$P = \frac{-V_{DS}\delta}{ARTt} \cdot \ln\left(\frac{p_{US} - p_{DS}}{P_{US}}\right)$$

where P is the permeability coefficient, V_{DS} is the downstream volume, δ is the film thickness, P_{us} is the upstream pressure, P_{DS} is the downstream pressure, A is the membrane area (m^2), R (m^3 Pa mol^{-1} K^{-1}) is the universal gas constant, T (K) is the absolute temperature, and t is time. A Fluke 700 GA6 digital pressure gauge provided pressure measurements with an accuracy of ±0.004 bar and the J-type thermocouple measured temperature with an accuracy of ±1 K.

For the pure component permeability measurements, the apparatus was evacuated to a pressure below 10^{-3} MPa for at least 12 h to remove any volatile impurities or residual solvent. Once degassing was complete, the gas was introduced into the upstream side of the membrane apparatus and maintained at a constant pressure of 2 bar. At this pressure, the fugacity coefficients are 0.97426 and 0.96856 for HFC-32 and HFC-125, respectively. These values, being close to 1, indicate that the system approximates ideal gas behavior under the applied conditions. Permeability measurements were conducted at room temperature. Selectivity of a given membrane was calculated by taking the ratio of HFC-32 permeability over the HFC-125 permeability.

Synthesis of sodium (2,4-difluorophenyl) ((trifluoromethyl) sulfonyl) amide IL [Na][DFPhTFMeSA] (anion precursor for M-2 and FIL-2). This compound was synthesized according to our previously established procedure.[29] A mixture of 2,4-difluoroaniline (7.6 mL, 75 mmol), triethylamine (10.5 g, 75 mmol), and chloroform (200 mL) was added to a three-necked round bottom flask equipped with an air condenser and an addition funnel under a nitrogen atmosphere. The reaction mixture was stirred at 0 °C for 15 minutes. Trifluoromethanesulfonic acid anhydride (12.65 g, 75 mmol) was placed in the addition funnel and added dropwise over the course of 1 h. The mixture was then refluxed for 1 h, allowed to cool to room temperature, and poured into 200 mL of water. The aqueous layer was extracted with chloroform (2 × 100 mL) then the combined chloroform extracts were dried over $MgSO_4$, filtered, and concentrated under reduced pressure. The resulting residue was suspended in an aqueous solution of 10 wt% NaOH and extracted with chloroform. The basic aqueous layer was filtered to remove solids and acidified with HCl, resulting in a solid precipitate. This precipitate was filtered and sublimed at 65 °C under static vacuum, then recrystallized from hexanes to yield a white crystalline solid (9.5 g, 55% yield). This compound (2.0 g, 8 mmol) was dissolved in anhydrous THF (10 mL) under nitrogen. Sodium metal (0.2 g, 8 mmol) was added, and the mixture was degassed by three freeze–pump–thaw cycles. The reaction was stirred at room temperature for 24 h or until sodium metal was no longer visible. Dichloromethane was added to precipitate the sodium salt, which was then isolated by vacuum filtration, yielding [Na][DFPhTFMeSA] (2.1 g, 92% yield). ^{1}H NMR (400 MHz, DMSO-d_6) δ 6.76 (m, 1H), 6.93 (m, 1H), 7.14 (m, 1H) ppm. ^{19}F NMR (376 MHz, DMSO-d_6) δ −76.27, −121.25, 122.03 ppm.

Synthesis of M-1 (3-(3,3,4,4,5,5,6,6,7,7,8,8,9,9,10,10,10-heptadecafluorodecyl)-1-vinyl-1*H*-imidazol-3-ium bis((trifluoromethyl)sulfonyl)amide). First, the cation was synthesized as an iodide salt by reacting 1-vinylimidazole (22 mmol, 1 equiv.) with 1*H*,1*H*,2*H*,2*H*-perfluodecyl iodide (24 mmol, 1.1 equiv.) in a Schlenk flask at 80 °C for 24 h under an inert atmosphere. After 24 h, the reaction mixture was dissolved in methanol then added to diethyl ether which resulted in precipitation. After three rounds of this purification (dissolution in minimal amount of methanol then precipitation in diethyl ether), the final product was isolated as a white powder in 66% yield. This iodide salt (1 equiv.) was dissolved in DCM and subjected to anion exchange with $LiTf_2N$ (1.1 equiv.), dissolved in water. The biphasic mixture was stirred for 24 h, resulting in formation of a precipitate. The solvent was decanted, and the solid was isolated and washed with water to remove any halide byproducts, resulting in a 90% yield. ^{1}H NMR (400 MHz, DMSO-d_6) δ 3.05 (m, 2H), 4.59 (t, 2H), 5.45 (dd, 1H), 5.97 (dd, 1H), 7.34 (dd, 1H), 8.01 (s, 1H), 8.21 (s, 1H), 9.56 (s, 1H) ppm. ^{19}F NMR (470 MHz, DMSO-d_6) δ −125.86, −123.26, −122.58, −121.79, −121.55, −113.22, −80.37, −78.84 ppm.

Synthesis of M-2 (3-(3,3,4,4,5,5,6,6,7,7,8,8,9,9,10,10,10-heptadecafluorodecyl)-1-vinyl-1*H*-imidazol-3-ium (2,4-difluorophenyl)((trifluoromethyl)sulfonyl)amide). The cation was synthesized as an iodide salt then anion exchange was performed between the iodide salt (1 equiv.) and [Na][DFPhTFMeSA] (1.1 equiv.), similar to as described above. Purification was performed as described above with M-2 isolated as a white gel in 92% yield. ^{1}H NMR (400 MHz, DMSO-d_6) δ 3.05 (m, 2H), 4.60 (t, 2H), 5.46 (dd, 1H), 5.97 (dd, 1H), 6.75 (m, 1H), 6.94 (m, 1H), 7.15 (m, 1H), 7.34 (dd, 1H), 8.02 (s, 1H), 8.21 (s, 1H), and 9.57 (s, 1H) ppm. ^{19}F NMR (470 MHz, DMSO-d_6) δ −125.78, −123.22, −122.50, −122.12, −121.71, −121.50, −121.33, −113.16, −80.28, −76.36 ppm.

Synthesis of M-3 (1-butyl-3-(2-(methacryloyloxy)ethyl)-1*H*-imidazol-3-ium bis((trifluoromethyl)sulfonyl)amide). M-3 was synthesized in three steps. First 2-bromoethyl methacrylate was synthesized by combining 2-bromoethanol (31.5 mmol, 1.05 eq.) and dichloromethane (5 mL) in a three-neck round bottom flask equipped with an addition funnel under N_2, cooled by an ice bath. A solution of triethylamine (33 mmol, 1.1 eq.) and dichloromethane (5 mL) was added to the flask and a solution of methacryloyl chloride (30 mmol, 1 eq.) in dichloromethane (5 mL) was added to the addition funnel then added to the flask dropwise. The resulting mixture was stirred for 24 h at room temperature, then filtered to remove salts. The filtrate (in dichloromethane) was washed with water four times and dried over magnesium sulfate. After filtration, solvent was removed under reduced pressure and the crude product was distilled at 70 °C to obtain 2-bromoethyl methacrylate as a clear liquid (70% yield). Next, 2-bromoethyl methacrylate (1 eq.) was reacted with butylimidazole (1.05 eq.) in a neat reaction at 40 °C for 24 h. A small amount of inhibitor (4-methoxyphenol) was added prior to running the reaction. After 24 h, the resulting viscous liquid was dissolved in a minimal amount of dichloromethane then added to diethyl ether which resulted in a precipitate. This process was repeated three times. The product, 1-butyl-3-(2-(methacryloyloxy)ethyl)-1*H*-imidazol-3-ium bromide, was isolated *via* centrifugation, as a viscous clear liquid in 65% yield. Finally, 1-butyl-3-(2-(methacryloyloxy)ethyl)-1*H*-imidazol-3-ium bromide (1 eq.) was dissolved in dichloromethane then an aqueous solution of lithium bistriflimide (1.05 eq.) was added. This biphasic mixture was stirred at room temperature for 24 h. The aqueous layer was then decanted, and the dichloromethane layer was concentrated under reduced pressure. The resultant viscous liquid was washed with water, until the water wash no longer tested positive for halides (*i.e.*, using an aqueous silver nitrate solution). Finally, M-3 was dried under vacuum and isolated in a 95% yield. ^{1}H NMR (400 MHz, DMSO-d_6) δ 0.88 (t, 3H), 1.23 (m, 2H), 1.75 (m, 2H), 1.84 (s, 3H), 4.19 (t, 2H), 4.48 (m, 2H), 4.51 (m, 2H), 5.71 (s, 1H), 6.02 (s, 1H), 7.70–7.82 (d, 2H), 9.24 (s, 1H) ppm. ^{19}F NMR (470 MHz, DMSO-d_6) δ −78.80 ppm.

Synthesis of FIL-1 and FIL-2. These ILs were synthesized as previously reported.[29,30] First, in an Ar filled glovebox 1-methylimidazole (12.5 mmol) was combined with 1*H*,1*H*,2*H*,2*H*-perfluorooctyl iodide (18.8 mmol, 1.5 equiv.) in a Schlenk flask. The flask was sealed, removed from the glovebox, connected to a Schlenk line, degassed, and fitted with an air condenser. The reaction mixture was kept under a nitrogen atmosphere and heated to 100 °C for 24 h, resulting in formation of a yellow solid and a clear liquid. Characterization of the crude mixture (both solid and liquid) using ^{1}H NMR spectroscopy showed the presence of the desired product as well as products from Hofmann elimination (*N*-methylimidazolium iodide and 1*H*,1*H*,2*H*-perfluoro-1-octene). The liquid layer, containing unreacted 1*H*,1*H*,2*H*,2*H*-perfluorooctyl iodide and 1*H*,1*H*,2*H*-perfluoro-1-octene, was removed with a pipette. The solid was washed with diethyl ether and dried under reduced pressure at 50 °C. To further purify, the solid was dissolved in a minimal amount of acetonitrile and filtered through a neutral alumina column, washing with toluene. The eluent was collected, and solvent was removed under reduced pressure at 50 °C overnight, yielding pure [(EtPFOctyl)MeIm][I].

FIL-1 and FIL-2 were synthesized through anion exchange between [(EtPFOctyl)MeIm][I] and the respective anion salt. For example, FIL-2 was synthesized by reacting sodium phenylsulfonamide (1.05 eq.) with [(EtPFOctyl)MeIm][I] (1 eq.) in water. The reaction mixture was stirred at room temperature for 24 h, resulting in formation of a viscous liquid beneath a less viscous aqueous phase. The aqueous phase was carefully decanted, and the non-aqueous layer washed with water. Each water wash was tested for halides using an aqueous silver nitrate solution. Once the silver nitrate test indicated the absence of halides, the viscous liquid was dried under vacuum overnight.

1-Methyl-3-(1H,1H,2H,2H-perfluorooctyl)-imidazolium bis(trifluoromethanesulfonyl)imide (FIL-1) was synthesized from [(EtPFHex)MeIm][I] and [Li][Tf_2N]. Red liquid (79%). ^{1}H NMR (400 MHz, DMSO-d_6) δ 2.99 (m, 2H), 3.87 (s, 3H), 4.56 (t, 2H), 7.71 (s, 1H), 7.86 (s, 1H), 9.19 (s, 1H) ppm. ^{19}F NMR (470 MHz, DMSO-d_6) δ −78.92, −80.53, −113.37, −121.85, −122.81, −123.37, −126.00 ppm. ^{13}C NMR (100 MHz, DMSO-d_6) δ137.7, 124.7, 124.1, 122.9, 121.5, 118.3, 115.1, 41.6, 36.2, 30.5 ppm.

1-Methyl-3-(1H,1H,2H,2H-perfluorooctyl)-imidazolium 2,4-difluorophenyl (trifluoromethylsulfonyl) amide (FIL-2) was synthesized from [(EtPFHex)MeIm][I] and [Na][DFPhTFMeSA]. Orange liquid (88%). ^{1}H NMR (400 MHz, DMSO-d_6) δ 3.00 (m, 2H), 3.87 (s, 3H), 4.56 (t, 2H), 6.75 (m, 1H), 6.92 (m, 1H), 7.15 (m, 1H), 7.72 (s, 1H), 7.87 (s, 1H), 9.20 (s, 1H) ppm. ^{19}F NMR (470 MHz, DMSO-d_6) δ −76.40, −80.35, −113.28, −121.35, −121.76, −122.07, −122.70, −123.28, −125.86 ppm. ^{13}C NMR (100 MHz, DMSO-d_6) δ157.3, 154.8, 137.7, 132.5, 127.5, 126.1, 124.1, 122.9, 120.9, 117.6, 115.9, 110.1, 103.5, 41.6, 36.3, 30.4 ppm.

Membrane preparation. The polymerizable FIL monomer (either M-1, M-2 or M-3) and the free IL (FIL-1, FIL-2, or FIL-3, respectively) were stirred with the appropriate amount of PEGDA crosslinker in a glass vial at room temperature. To this, the photoinitiator DMPA (1 wt%) was added and the solution stirred for 1 h. The resulting homogeneous solution was subjected to ultrasonication for 1 h at room temperature to eliminate entrapped air bubbles. Subsequently, the mixture was carefully pipetted onto a quartz glass slide that had been precoated with either a PTFE dry spray or Rain-X. This coating on the glass slide provided a hydrophobic surface, facilitating the removal of the membrane. Another coated glass slide was placed on top, sandwiching the pipetted mixture. The gap between the glass slides was adjusted using a spacer with a thickness of ~110 μm. The plates were then placed under a UV lamp (365 nm, 9 W) for ~1 h. Post irradiation, the glass slides were separated using a clean razor blade and the composite membrane was peeled off. The thickness of the membranes was determined to be 100–120 μm using a vernier caliper. A

Table 1 Membrane compositions using M-1, M-2, and M-3. $T_{5\%}$ indicates the temperature at which 5% mass loss is observed and T_g is the glass transition temperature

Monomer type	Crosslinker (CL) PEGDA (M_n = 575 or M_n = 250)	Free IL	Membrane name [monomer][crosslinker$_{wt\%}$][free IL$_{eq.}$]	$T_{5\%}$[a] (°C)	T_g[b] (°C)
Monomer-1 (M-1)	50 wt% (M_n = 575)	1 eq.	[M-1][CL_{50}][FIL-1_1]	294	−10.5
	50 wt% (M_n = 575)	0.5 eq.	[M-1][CL_{50}][FIL-$1_{0.5}$]	286	−5.5
	50 wt% (M_n = 575)	—	[M-1][CL_{50}]	283	−0.8
	70 wt% (M_n = 575)	1 eq.	[M-1][CL_{70}][FIL-1_1]	296	−14.1
Monomer-2 (M-2)	50 wt% (M_n = 575)	1 eq.	[M-2][CL_{50}][FIL-2_1]	210	−7.5
	50 wt% (M_n = 575)	0.5 eq.	[M-2][CL_{50}][FIL-$2_{0.5}$]	205	−5.4
	50 wt% (M_n = 575)	—	[M-2][CL_{50}]	200	−1.8
Monomer-3 (M-3)	20 wt% (M_n = 250)	1 eq.	[M-3][CL_{20}][FIL-3_1]	355	−30.4

[a] Determined by thermogravimetric analysis (TGA). [b] Determined by differential scanning calorimetry (DSC).

summary of the compositions of the materials investigated in this work is given in Table 1.

3. Results and discussion

Design and synthesis of fluorinated poly(IL) membranes

A series of poly(IL)-IL membranes were synthesized utilizing two IL monomers with cations and anions that are fluorinated, and one IL monomer with a non-fluorinated cation and a fluorinated anion; Fig. 1 illustrates the naming convention and structures of the different monomers and FILs employed for membrane fabrication. The syntheses of these monomers and FILs involved the preparation of halide salts of the cations and sodium salts of the anions, followed by ion exchange. M-1 and M-2 were synthesized from the iodide salt of the cation by reaction of vinylimidazole with 1*H*,1*H*,2*H*,2*H*-perfluorodecyl iodide. To prepare the cation for FIL-1 and FIL-2, methylimidazole was reacted with 1*H*,1*H*,2*H*,2*H*-perfluorooctyl iodide. Subsequently, anion exchange with lithium bistriflimide produced M-1 and FIL-1. To prepare M-2 and FIL-2, the (2,4-difluorophenyl) ((trifluoromethyl)sulfonyl) amide anion was prepared as a sodium salt, followed by ion exchange with the imidazolium cation. The synthesis of the methacrylate-based M-3 was inspired by previously reported methodologies,[27,31] with anion exchange performed using lithium bistriflimide. The IL monomers were designed to investigate the influence of the polymer composition on the physicochemical and gas transport properties of the membranes, as the pendant groups are expected to dictate van der Waals interactions and free volume. The FILs were designed for consistent chemical composition within each membrane (*e.g.*, prevent phase separation).

Poly(IL)-IL membranes were fabricated by UV-photopolymerization of cast films (Fig. 2), a widely employed technique used to prepare membranes for CO_2 separation.[24,32–34] Here, membranes from four formulations using M-1, three formulations using M-2, and one formulation of M-3 were prepared and evaluated. For these formulations, varying amounts of free IL were incorporated: 1, 0.5, and 0 equivalents. The membrane nomenclature is defined as [monomer][crosslinker$_{wt\%}$][free IL$_{eq.}$], where each component specifies the monomer type, the weight percentage of the crosslinker, and the equivalents of free IL, respectively. After testing various combinations *via* trial-and-error, free-standing membranes from M-1 and M-2 were determined to require 50 wt% of the PEGDA crosslinker with a molar mass of 575 Da (Table 1). In contrast, using M-3 only 20 wt% of a lower molar mass PEGDA cross-linker (M_n = 250 Da) was required to form free-standing membranes (Table 1). For all formulations, 1 wt% of the photoinitiator DMPA was used. The difference in the crosslinking requirements between the fluorinated and non-fluorinated systems is likely due to differences in molecular interactions introduced by fluorination (*e.g.*, collective van der Waals interactions). Fluorinated monomers and ILs are known to create a more rigid and less flexible polymer matrix (with larger free volume), thus necessitating greater amounts of crosslinker to achieve a stable and free-standing

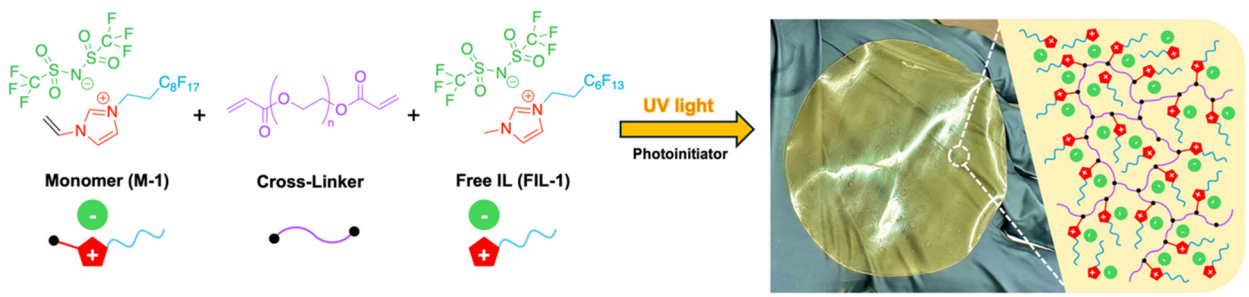

Fig. 2 Illustration of composite poly(IL)-IL membrane preparation. Photograph on the right shows a freestanding membrane held in a gloved hand.

membrane; in contrast, non-fluorinated systems are more flexible and require less crosslinking to achieve the same membrane properties.[35,36] All poly(IL)-IL membranes were soft and flexible structures, similar to commonly used polydimethylsiloxane (PDMS) membranes, and were sufficient for gas permeation testing (Fig. 2 and Fig. S3†).

Structural characterization of the fluorinated membranes

Fourier-transform infrared (FTIR) spectroscopy was used to qualitatively characterize the composition of the membranes. As depicted in Fig. 3, characteristic C=C stretching frequencies at 1635 and 1617 cm^{-1} associated with the terminal vinyl ester of the PEGDA crosslinker, as well as that of M-1 around 1640 cm^{-1} are not present in the spectra of the membranes, indicating consumption of these reactive groups upon polymerization. This is further supported by the disappearance of $=CH_2$ bending frequencies at 985 cm^{-1} for the crosslinker and at 996 and 929 cm^{-1} for M-1. Additionally, a shift of the strong signal corresponding to C=O of the PEGDA crosslinker from 1718 to 1734 cm^{-1} was observed upon membrane formation, supporting consumption of the α,β-unsaturated ester. Comparison of the FTIR spectra of M-1 and the membrane [M-1][CL_{50}][FIL-1_1] provides additional confirmation of the successful formation of the poly(IL)-IL membranes. For instance, the C–N vibrational modes of the imidazolium cation of M-1 appear around 1330 cm^{-1} in the spectrum of [M-1][CL_{50}][FIL-1_1]. Further, features indicative of the presence of Tf_2N anions are observed at 1176 cm^{-1} for SO_2 stretching, 1055 cm^{-1} for SNS stretching, and from 500–600 cm^{-1} for C–F stretching. Similar observations are evident in the FTIR spectra of membranes synthesized with M-2 (Fig. S1†) and M-3 (Fig. S2†), with the most significant being the disappearance of the C=C stretching frequencies at 1640 cm^{-1} for M-2 and 1635 cm^{-1} for M-3, indicating complete consumption of monomer and cross-linker in these formulations as well. In addition to FTIR analysis, ^1H NMR of membrane extracts in DMSO-d_6 with mesitylene as an internal standard (0.012 M) showed no detectable signals from unreacted monomers or crosslinker (Fig. S8–S10†). This indicates the absence of extractable unreacted monomers and crosslinkers and thus their successfully incorporated into the polymer network.

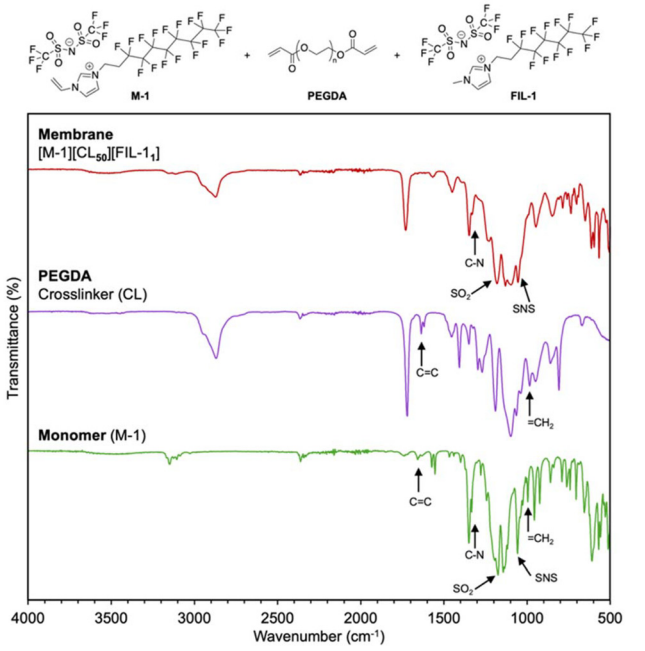

Fig. 3 FTIR spectra of M-1, PEGDA, and poly(IL)-IL membrane [M-1][CL_{50}][FIL-1_1].

Thermal stability of poly(IL)-IL membranes

The thermal stability of all membranes was assessed by thermogravimetric analysis (TGA). The weight loss profiles of M-1 and M-2 membranes showed three-stage decomposition, consistent with previous reports on the thermal stability of poly(IL)-IL membranes.[24] To facilitate comparison of the composite membranes, the temperature at which 5% mass loss occurred was used ($T_{5\%}$). As illustrated in Fig. 4A, the $T_{5\%}$ for M-1 membranes ranged from 286 to 296 °C with that of [M-1][CL_{50}][FIL-1_1] (294 °C) being higher than that of [M-1][CL_{50}][FIL-$1_{0.5}$] (286 °C); this suggests that less free IL reduces thermal stability. This difference may be attributed to the reduced electrostatic interactions between the free IL and polymer chains within the crosslinked matrix with decreasing amount of free IL. Furthermore, [M-1][CL_{70}][FIL-1_1], a membrane with a higher amount of crosslinker, exhibited a slightly elevated $T_{5\%}$ (296 °C) compared to the membrane with less cross-linking ([M-1][CL_{50}][FIL-1_1], 294 °C). Similar trends in thermal stability were observed for the M-2-based membranes (Fig. S4†).

The $T_{5\%}$ for [M-1][CL_{50}][FIL-1_1] and [M-2][CL_{50}][FIL-2_1] were 294 °C and 210 °C, respectively (Fig. 4B, Table 1). These membranes have the same density of cross-linking, however, the M-2 membrane exhibited significantly lower thermal stability than the M-1 membrane, highlighting the substantial impact of the anion on thermal stability. Our previous studies demonstrated that the thermal stability of FIL-2 was approximately 240 °C, whereas that of FIL-1 was about 280 °C.[29] This disparity was attributed to weaker anion–cation interactions in FIL-1, resulting from charge delocalization across the Tf_2N ion, reducing its nucleophilicity and affecting the primary decomposition steps involving nucleophilic substitution.[37,38] Therefore, the lower thermal stability of [M-2][CL_{50}][FIL-2_1] is possibly due to the relatively increased nucleophilicity of the anion of M-2 and FIL-2.

The methacrylate-based [M-3][CL_{20}][FIL-3_1] membrane, which contains a 1 : 1 composition of the partially fluorinated M-3 and FIL-3, demonstrated significantly higher thermal stability ($T_{5\%}$ = 354 °C) compared to the two fully fluorinated membranes, [M-1][CL_{50}][FIL-1_1] and [M-2][CL_{50}][FIL-2_1] (Fig. S5†). This enhanced thermal stability may be attributed to the higher $T_{5\%}$ of FIL-3, [C_6C_1im][Tf_2N] (305 °C). The stronger C–N bond between the imidazolium ring and the non-

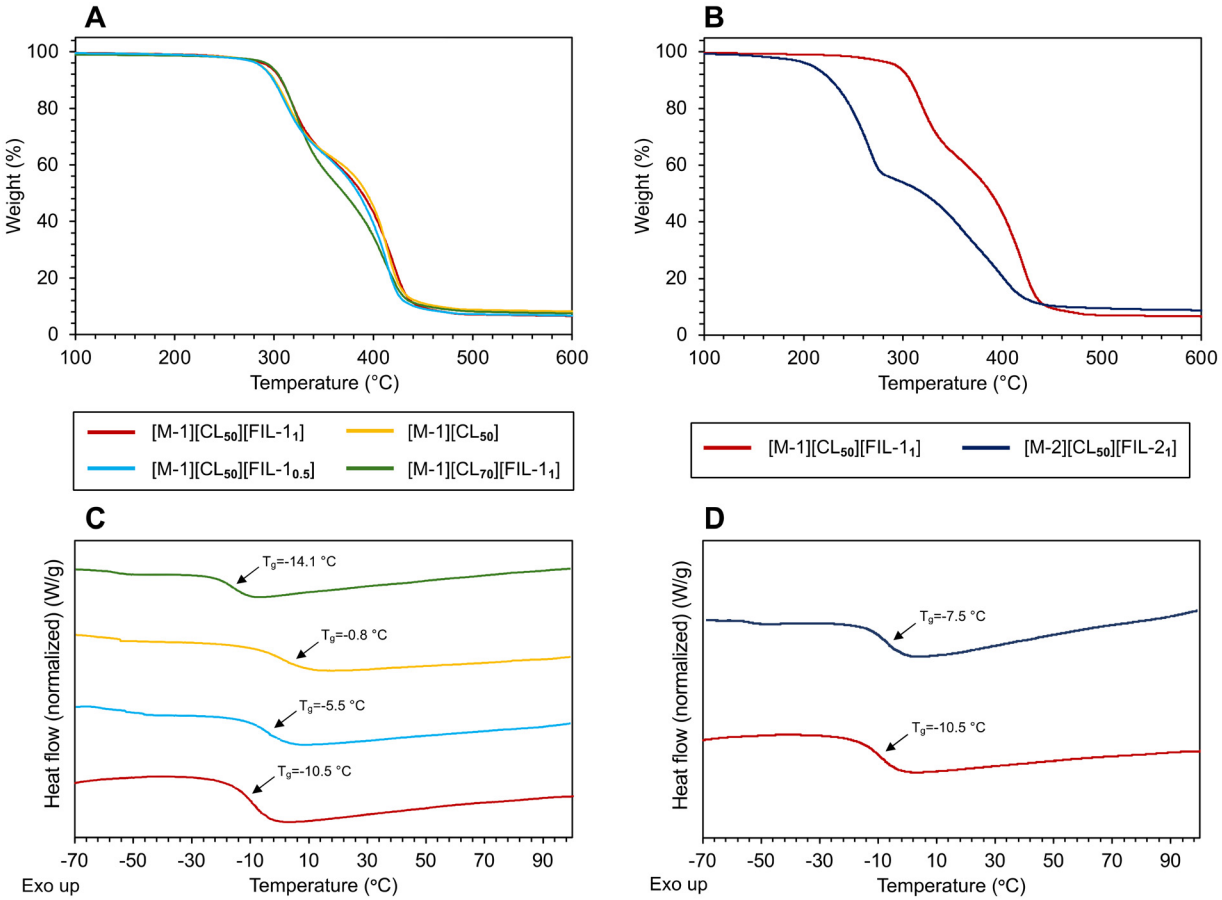

Fig. 4 (A) Thermal weight loss profiles of membranes prepared from M-1. (B) Comparison of thermal weight loss profile of [M-1][CL_{50}][FIL-1_1] and [M-2][CL_{50}][FIL-2_1]. (C) Second heating cycle of the DSC thermogram of poly(IL)-IL membranes prepared from M-1. (D) Second heating cycle of the DSC profile comparing [M-1][CL_{50}][FIL-1_1] and [M-2][CL_{50}][FIL-2_1].

fluorinated alkyl chain in FIL-3, compared to that of the highly fluorinated chain of FIL-1 and FIL-2, may increase the energy required for the nucleophilic substitution as a decomposition step, thus elevating $T_{5\%}$. Regardless, all poly(IL)-IL composite membranes had $T_{5\%}$ > 200 °C, making them suitable for membrane-based gas separation applications under typical operating temperatures.

Thermal behavior of the fluorinated membranes

The thermal phase transitions of all membranes were examined using differential scanning calorimetry (DSC). As detailed in Table 1, all composite membranes exhibited a single glass transition temperature (T_g) below 0 °C, thus making them rubbery at ambient temperatures. Fig. 4C illustrates the second-cycle DSC heating curves of the four membranes prepared from M-1, varying in cross-link density and loading of free IL. The T_g values for [M-1][CL_{50}][FIL-1_1], [M-1][CL_{50}][FIL-$1_{0.5}$], and [M-1][CL_{50}] increased with decreased free IL and are −10.5 °C, −5.5 °C, and −0.8 °C, respectively. Free IL typically function as plasticizers in polymer membranes, enhancing the free volume and molecular mobility of the polymer chains, which results in a lowering of the T_g. Interestingly, for [M-1][CL_{70}][FIL-1_1], the T_g decreased to −14.1 °C with the inclusion of 70 wt% crosslinker, which was unexpected as T_g typically increases with increasing cross-linking density. This anomaly may be due to the lower T_g of the PEGDA network (T_g = −25 °C for crosslinked pure PEGDA with M_n = 575 Da).[39] A similar trend was observed for the T_g values of the membranes based on M-2 (Fig. S6†), increasing with decreasing free IL content.

Fig. 4D shows the T_g values for membranes with the same amount of cross-linker but different monomer and free IL (*i.e.*, [M-1][CL_{50}][FIL-1_1] and [M-2][CL_{50}][FIL-2_1]), which are −10.5 °C and −7.5 °C, respectively. The higher T_g value observed for [M-2][CL_{50}][FIL-2_1] may be attributed to stronger intermolecular interactions within the crosslinked network, such as π–π interactions resulting from the aromatic anion, which reduce the segmental motion of the polymer chains and slightly increases T_g. In contrast, the methacrylate-based [M-3][CL_{20}][FIL-3_1] shows a significantly lower T_g of −30.4 °C (Fig. S7†). This decrease in T_g can be explained by the presence of the more flexible non-fluorinated alkyl chains in both the monomer and the free IL, combined with the plasticizing effect of the IL, which together enhance chain mobility within

the polymer network. Furthermore, a lower loading and lower molar mass (20 wt% of M_n = 250 Da) of crosslinker was required, which also contribute to the reduced T_g.

Gas separation performance

To the best of our knowledge, this is the first study to report HFC gas permeation in fluorinated composite poly(IL)-IL membranes, as to date most studies have focused on the use of amorphous perfluoropolymer membranes.[8,9] Gas permeability in polymeric membranes, based on the solution–diffusion mechanism for the separation of gas mixtures, is primarily governed by the solubility and diffusivity of the gases.[40] In amorphous polymer membranes such as those reported herein, gas permeation is largely dictated by the characteristics of the penetrant gas, such as size and critical volume, by polymer properties like T_g, free volume, and van der Waals interactions between the polymer and the penetrant.[40] The poly(IL)-IL composite membranes containing rigid fluorinated pendant groups are proposed to enhance the permeability of HFC gases due to the increased free volume of the polymer, which should increase diffusivity, as well as the favorable van der Waals interactions between fluorinated alkyl chains and HFC gases, which increase solubility. Table 2 presents the permeability data for HFC-32 and HFC-125 for the different membrane compositions discussed above.

Among the various membrane compositions of M-1, [M-1][CL_{50}][FIL-1_1] exhibited the highest HFC-32 permeability of 55 Barrer. A progressive decline in the permeability of HFC-32 was observed with decreasing free IL content of the membrane. Notably, [M-1][CL_{50}] with no free IL demonstrated the lowest HFC-32 permeability. This trend aligns with the understanding that free IL within the polymer matrix enhances the mobility and spacing of polymer chains through plasticization, a phenomenon consistent with prior studies showing decreased CO_2 permeability with reduced free IL content.[24,34,41] Notably, [M-1][CL_{70}][FIL-1_1], with a higher crosslinker content (70 wt%), demonstrated a permeability for HFC-32 of 19.2 Barrer. This indicates that an increase in crosslinking density leads to reduced permeability, attributed to the restricted polymer chain mobility, which consequently decreases the diffusivity of gases through the membrane. However, the reduction in permeability was less pronounced compared to [M-1][CL_{50}][FIL-$1_{0.5}$], which had an HFC-32 permeability of 15.3 Barrer. This suggests that a sufficient amount of free IL may still enhance chain mobility and gas diffusivity, despite the higher crosslinking density, providing multiple variables to tune for optimal performance.

Further analysis of the permeability results can be made based on the T_g values of the membranes (Table 2). There is a direct correlation between T_g and the free volume within a composite poly(IL)-IL membrane;[24] as T_g decreases, the free volume typically increases, resulting in greater molecular mobility and potentially enhanced gas permeability. Based on this relationship, the lower T_g of [M-1][CL_{70}][FIL-1_1] (−14.1 °C) compared to [M-1][CL_{50}][FIL-1_1] (−10.5 °C), suggests that the former should exhibit higher permeability due to enhanced gas diffusivity and higher free volume, but this is not observed. This anomaly indicates the crucial role of interactions between HFC gases and the polymer in gas uptake, highlighting that permeability is also influenced by solubility, or that the difference in free volume (*i.e.*, T_g) is not large enough for appreciable differences to be observed. Previous reports have shown that HFC gases can form hydrogen bonds with the fluorinated components of an IL, aiding their uptake. Thus, we hypothesize that increased crosslinking density might hinder the effective interaction of the fluorinated moieties of both the polymer pendants and free IL with HFC gases, thereby reducing their solubility in the polymer membrane, resulting in decreased overall permeability.

Comparing HFC-32 permeability of [M-2][CL_{50}][FIL-2_1] (22.0 Barrer) with [M-1][CL_{50}][FIL-1_1] (55.0 Barrer), the significantly higher permeability of the latter is consistent with the expectation based on T_g. The higher T_g of [M-2][CL_{50}][FIL-2_1] (−7.5 °C) indicates a more rigid polymer network, suggesting lower HFC gas permeability due to differences in both gas diffusivity and solubility. A similar permeability trend of decreasing gas permeability with decreasing free IL content was observed between [M-2][CL_{50}][FIL-2_1] and [M-2][CL_{50}]. It is important to note that gas permeability of [M-2][CL_{50}][FIL-$2_{0.5}$] was not measured due to its lack of mechanical stability (*i.e.*, the samples tore when loading). Interestingly, [M-3][CL_{20}][FIL-3_1] exhibited an unexpectedly high HFC-32 permeability of 53 Barrer. Given the structural composition, specifically the absence of fluorinated alkyl chains, a lower gas permeability compared to the highly fluorinated membranes was anticipated. However, the substantial increase in permeability can be attributed to the enhanced diffusivity of the HFC-32 gas, which is likely due to increased chain mobility resulting from the greater flexibility in the non-fluorinated polymer chains as well as lower crosslinking density. This observation is consistent with the much lower T_g of −30.4 °C.

For all membranes, HFC-32 had higher permeability than HFC-125. This difference can be attributed to its smaller molecular size of HFC-32, resulting in higher diffusivity relative to the larger HFC-125.[9] Previous studies on the permeability of various gases using polymeric membranes demonstrated a

Table 2 HFC-32 and HFC-125 gas permeabilities and selectivities[a]

Membrane name	HFC-32 permeability	HFC-125 permeability	Selectivity
[M-1][CL_{50}][FIL-1_1]	55.0 ± 5.5	5.85 ± 0.6	9.5 ± 1.3
[M-1][CL_{50}][FIL-$1_{0.5}$]	15.3 ± 1.5	2.6 ± 0.7	5.9 ± 1.8
[M-1][CL_{50}]	11.3 ± 1.1	1.1 ± 0.1	10.2 ± 1.6
[M-1][CL_{70}][FIL-1_1]	19.2 ± 1.9	1.1 ± 0.1	19.2 ± 2.8
[M-2][CL_{50}][FIL-2_1]	22.0 ± 2.2	2.0 ± 0.2	11.0 ± 1.6
[M-2][CL_{50}]	18.2 ± 1.8	1.2 ± 0.1	15.1 ± 2.3
[M-3][CL_{20}][FIL-3_1]	53.0 ± 5.3	4.5 ± 0.5	11.8 ± 1.7

[a] The permeability of [M-2][CL_{50}][FIL-$2_{0.5}$] was not tested as the membrane was not mechanically stable for testing.

general decrease in permeability with increasing critical volume of the gas, highlighting the critical role of diffusivity in determining permeability.[9] HFC-125 permeability exhibited similar trends to that of HFC-32, where permeability decreased with decreasing loading of free IL, and the highest permeability of HFC-125 was achieved using [M-1][CL_{50}][FIL-1_1]. When comparing [M-1][CL_{50}][FIL-1_1] with [M-2][CL_{50}][FIL-2_1], the same trend with HFC-32 is observed: the permeability of HFC-125 in [M-1][CL_{50}][FIL-1_1] (5.85 Barrer) is higher than in [M-2][CL_{50}][FIL-2_1] (2.0 Barrer), which can be attributed to the reduced free volume caused by the bulkier anion. HFC-125 permeability through [M-3][CL_{20}][FIL-3_1] also follows the same trend as HFC-32, being higher than in some of the fully fluorinated membranes.

The highest selectivity observed was 19.2 with [M-1][CL_{70}][FIL-1_1], despite the relatively low permeability for both gases in this membrane but with slower diffusion of HFC-125 through the more heavily crosslinked polymer network. Conversely, the membrane with lower crosslinking but the same monomer and free IL, [M-1][CL_{50}][FIL-1_1], exhibited a much lower selectivity (9.5) but with the highest permeability for both HFC-32 (55 Barrer) and HFC-125 (5.85 Barrer). These findings suggest a complex interplay between the solubility and diffusivity of the gases, warranting further studies to fully deconvolute the relationship.

Printing of composite membranes

Digital light processing (DLP) additive manufacturing has recently garnered significant attention due to its versatility in quickly prototyping membranes of complex, customized geometries.[42–46] This technology has also been developed to enable the one-step fabrication of solid–liquid composites.[42,47,48] Unlike traditional methods that require vacuum-filling of porous scaffolds, DLP minimizes liquid material waste and streamlines the fabrication process to essentially a single step.[49–51] We hypothesized that the poly(IL)-IL composites could be formulated for DLP vat photopolymerization provided development of an appropriate photosensitive resin. Indeed, DLP is particularly effective for printing composites containing monomers with electron-deficient double bonds as it involves curing thin layers sequentially, ensuring polymerization of each layer and reducing the risk of incomplete curing or defects.[49]

For printing, the formulation utilized for the membrane [M-1][CL_{50}][FIL-1_1] was used. We substituted the photoinitiator DMPA with phenylbis(2,4,6-trimethylbenzoyl)phosphine oxide (BAPO) to align with the 405 nm wavelength of the printer. The resin was loaded into the vat, and UV light was used to cure the material based on pre-sliced models (layer height of 100 μm), creating 3D structures as the build platform incre-

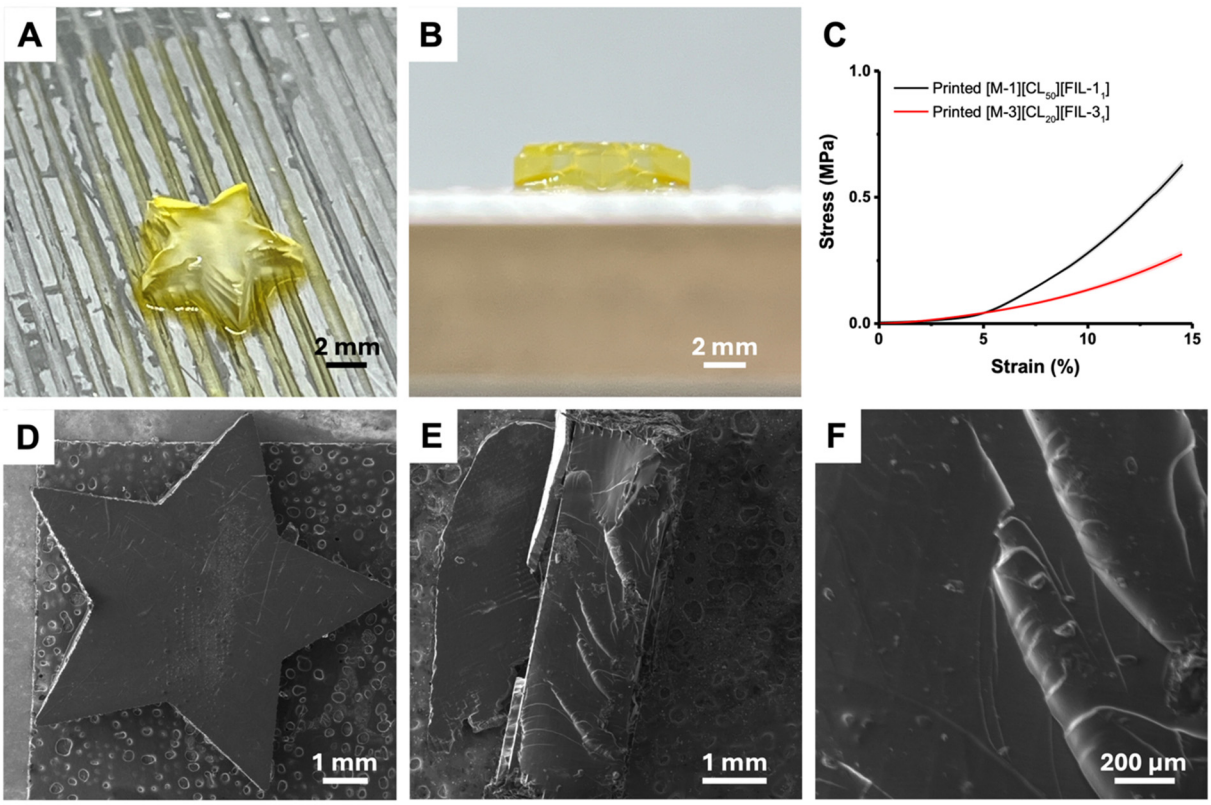

Fig. 5 Images of [M-1][CL_{50}][FIL-1_1] printed by digital light processing (DLP): (A) on build platform from the top and (B) from the side. (C) Stress–strain curve from the DMA compression test of both [M-1][CL_{50}][FIL-1_1] and [M-3][CL_{20}][FIL-3_1]. SEM images: (D) top view, (E) cross-section, and (F) cross-section magnification.

mentally elevated. To assess the formulation's capability for high-resolution printing, we designed a star-shaped structure. As depicted in Fig. 5A, the printed object achieved excellent resolution with a uniform height (Fig. 5B). The model had an end-to-end length of 7.8 mm and a thickness of 2.0 mm, and the printed object exhibited nearly identical dimensions, demonstrating its excellent resolution and minimum shrinkage. As common practice for DLP-produced objects, the prints were subjected to one minute of post-curing with UV light.

The mechanical properties of the printed poly(IL)-IL part were evaluated using dynamic mechanical analysis (DMA) in compression mode. As shown in Fig. 5C, the stress–strain curve exhibited two distinct regions: an initial compressive modulus of ~0.50 MPa for strains between 0–4%, likely attributable to the redistribution of free IL, followed by a much higher average compressive modulus of 5.92 MPa, which can be attributed to the crosslinked polymer network. This compression test was conducted three times, with high reproducibility. Notably, the test was terminated at 14.5% strain upon reaching the instrument's force limit of 20 N. For comparison, the non-fluorinated membrane [M-3][CL_{20}][FIL-3_1] was also fabricated by DLP, and its stress–strain behavior is presented in Fig. 5C. This formulation could be printed, as anticipated, and the mechanical properties were significantly softer, exhibiting a compressive modulus of 3.05 MPa. This reduction in mechanical performance is attributed to its lower crosslinking density and the increased flexibility of the resulting polymer network. We examined the surface and cross-sectional characteristics of the printed [M-1][CL_{50}][FIL-1_1] object using scanning electron microscopy (SEM). Fig. 5D shows that the sample has no surface defects and confirms that the DLP system's resolution limit of approximately 50 μm was achieved. The cross-sectional view (Fig. 5E and F) revealed a homogeneous composite without noticeable phase separation. This uniformity, coupled with the high-resolution printability and robust mechanical properties, highlights the potential of 3D printing composite membranes as a rapid membrane fabrication method for various applications.

4. Conclusions

In this study, we developed fluorinated poly(IL)-IL composite membranes and evaluated their thermal properties and permeability to two different refrigerant gases. The primary objective was to investigate the influence of fluorinated pendant moieties on the physical properties and gas separation performance of these membranes. Two types of vinyl-based fluorinated IL monomers (M-1 and M-2) and a methacryloxy-based IL monomer (M-3) were synthesized and used to formulate the membranes, with PEGDA used as a crosslinker to enhance mechanical stability. Membranes were produced by UV curing and characterization *via* FTIR spectroscopy confirmed polymerization of monomer and cross-linker. The membranes had good thermal stability with $T_{5\%}$ ranging from 286 to 354 °C, making them suitable under common operating conditions. DSC analysis demonstrated that all T_g values were below 0 °C but depended on the monomer, amount of crosslinker, and free IL content. The inclusion of free IL acted as a plasticizer, increasing free volume and molecular mobility, thereby reducing T_g.

Gas permeability tests indicated that the fluorinated poly(IL)-IL composite membranes have promising performance for HFC gas separation. Notably, all membranes exhibited higher permeability for HFC-32 than HFC-125, which was attributed to the smaller molecular size and higher diffusivity of HFC-32. Among the membranes studied, [M-1][CL_{50}][FIL-1_1] displayed the highest HFC-32 permeability, while [M-3][CL_{20}][FIL-3_1] showed high permeability due to increased chain flexibility and free volume within the polymer matrix. [M-1][CL_{70}][FIL-1_1] had the highest ideal selectivity observed, 19.2. Lastly, we demonstrate the ability to print the composite membranes by DLP which demonstrates the opportunity to rapidly fabricate composite membranes with excellent resolution, uniformity, and robust mechanical properties. Overall, this work provides valuable insights into the design and synthesis of poly(IL)-IL composite membranes and their potential applications in gas separation. Future studies will focus on varying membrane formulations to achieve higher permeability and selectivity of the HFC gases for application in refrigerant recycling and leveraging other printing techniques such as projection microstereolithography or two-photon polymerization to enhance resolution.

Conflicts of interest

The authors declare no conflict of interest.

Data availability

The authors declare that all data supporting this manuscript are available upon reasonable request.

Acknowledgements

This work was supported by the National Science Foundation (NSF) award number 2029354 through the Emerging Frontier in Research Innovation (EFRI) DChem program and the Welch Foundation Grant A-2117-2022033.

References

1 J. E. Sosa, R. Santiago, A. E. Redondo, J. Avila, L. F. Lepre, M. C. Gomes, J. M. M. Araújo, J. Palomar and A. B. Pereiro, Design of Ionic Liquids for Fluorinated Gas Absorption: COSMO-RS Selection and Solubility Experiments, *Environ. Sci. Technol.*, 2022, **56**(9), 5898–5909, DOI: **10.1021/acs.est.2c00051**.

2 C. S. M. Kang, X. Zhang and D. R. MacFarlane, Synthesis and Physicochemical Properties of Fluorinated Ionic Liquids with High Nitrogen Gas Solubility, *J. Phys. Chem. C*, 2018, **122**(43), 24550–24558, DOI: 10.1021/acs.jpcc.8b07752.

3 L. F. Lepre, D. Andre, S. Denis-Quanquin, A. Gautier, A. A. H. Pádua and M. Costa Gomes, Ionic, Liquids Can Enable the Recycling of Fluorinated Greenhouse Gases, *ACS Sustainable Chem. Eng.*, 2019, **7**(19), 16900–16906, DOI: 10.1021/acssuschemeng.9b04214.

4 J. E. Sosa, R. P. P. L. Ribeiro, P. J. Castro, J. P. B. Mota, J. M. M. Araújo and A. B. Pereiro, Absorption of Fluorinated Greenhouse Gases Using Fluorinated Ionic Liquids, *Ind. Eng. Chem. Res.*, 2019, **58**(45), 20769–20778, DOI: 10.1021/acs.iecr.9b04648.

5 US EPA, O. *Overview of Greenhouse Gases*. https://www.epa.gov/ghgemissions/overview-greenhouse-gases (accessed 2024-05-29).

6 K. R. Baca, G. M. Olsen, L. Matamoros Valenciano, M. G. Bennett, D. M. Haggard, B. J. Befort, A. Garciadiego, A. W. Dowling, E. J. Maginn and M. B. Shiflett, Phase Equilibria and Diffusivities of HFC-32 and HFC-125 in Ionic Liquids for the Separation of R-410A, *ACS Sustainable Chem. Eng.*, 2022, **10**(2), 816–830, DOI: 10.1021/acssuschemeng.1c06252.

7 A. R. C. Morais, A. N. Harders, K. R. Baca, G. M. Olsen, B. J. Befort, A. W. Dowling, E. J. Maginn and M. B. Shiflett, Phase Equilibria, Diffusivities, and Equation of State Modeling of HFC-32 and HFC-125 in Imidazolium-Based Ionic Liquids for the Separation of R-410A, *Ind. Eng. Chem. Res.*, 2020, **59**(40), 18222–18235, DOI: 10.1021/acs.iecr.0c02820.

8 A. N. Harders, E. R. Sturd, L. Wallisch, H. Schmidt, Y. Mendoza-Apodaca, D. R. Corbin, W. White, C. P. Junk and M. B. Shiflett, Solubility, Diffusivity, and Permeability of HFC-32 and HFC-125 in Amorphous Copolymers of Perfluoro(Butenyl Vinyl Ether) and Perfluoro(2,2-Dimethyl-1,3-Dioxole), *Ind. Eng. Chem. Res.*, 2023, **62**(9), 4054–4063, DOI: 10.1021/acs.iecr.2c04518.

9 A. N. Harders, E. R. Sturd, J. E. Vallier, D. R. Corbin, W. R. White, C. P. Junk and M. B. Shiflett, Selective Separation of HFC-32 from R-410A Using Poly (Dimethylsiloxane) and a Copolymer of Perfluoro(Butenyl Vinyl Ether) and Perfluoro(2,2-Dimethyl-1,3-Dioxole), *J. Membr. Sci.*, 2022, **652**, 120467, DOI: 10.1016/j.memsci.2022.120467.

10 Yu. Yampolskii, N. Belov and A. Alentiev, Perfluorinated Polymers as Materials of Membranes for Gas and Vapor Separation, *J. Membr. Sci.*, 2020, **598**, 117779, DOI: 10.1016/j.memsci.2019.117779.

11 K. Friess, P. Izák, M. Kárászová, M. Pasichnyk, M. Lanč, D. Nikolaeva, P. Luis and J. C. Jansen, A Review on Ionic Liquid Gas Separation Membranes, *Membranes*, 2021, **11**(2), 97, DOI: 10.3390/membranes11020097.

12 R. Nasir, D. F. Mohshim, H. A. Mannan, D. Qadir, H. Mukhtar, K. Maqsood, A. Ali, B. Maulianda, A. Abdulrahman and A. B. Mahfouz, A Perspective on Ionic Liquid-Based Membranes for CO2 Separation, *Chem. Pap.*, 2021, **75**(3), 839–852, DOI: 10.1007/s11696-020-01384-y.

13 G. P. Dennis, K. E. O'Harra, X. Liu, E. M. Jackson, C. H. Turner and J. E. Bara, Experimental and Computational Studies on the Effects of C(2) Methylation on the Properties and Gas Separation Performance of Polyimide-Ionene Membranes, *RSC Appl. Polym.*, 2023, **1**(1), 111–122, DOI: 10.1039/D3LP00092C.

14 H. Karkhanechi, S. Salmani and M. Asghari, A Review on Gas Separation Applications of Supported Ionic Liquid Membranes, *ChemBioEng Rev.*, 2015, **2**(4), 290–302, DOI: 10.1002/cben.201500001.

15 X. J. Yang, A. G. Fane and K. Soldenhoff, Comparison of Liquid Membrane Processes for Metal Separations: Permeability, Stability, and Selectivity, *Ind. Eng. Chem. Res.*, 2003, **42**(2), 392–403, DOI: 10.1021/ie011044z.

16 J. E. Bara, C. J. Gabriel, T. K. Carlisle, D. E. Camper, A. Finotello, D. L. Gin and R. D. Noble, Gas Separations in Fluoroalkyl-Functionalized Room-Temperature Ionic Liquids Using Supported Liquid Membranes, *Chem. Eng. J.*, 2009, **147**(1), 43–50, DOI: 10.1016/j.cej.2008.11.021.

17 T. Patil, S. Dharaskar, M. Sinha and S. S. Jampa, Effectiveness of Ionic Liquid-Supported Membranes for Carbon Dioxide Capture: A Review, *Environ. Sci. Pollut. Res.*, 2022, **29**(24), 35723–35745, DOI: 10.1007/s11356-022-19586-0.

18 T. Patil, S. Dharaskar, M. K. Sinha, J. Pandya, S. Shinde, S. S. Kumar Jampa, M. Sillanpaa and C. Yoo, Efficient CO2/CH4 Separation Using [Bmim][Ac]/Pebax-1657 Supported Ionic Liquid Membranes and Its Prediction by Density Functional Theory, *Int. J. Greenhouse Gas Control*, 2023, **124**, 103856, DOI: 10.1016/j.ijggc.2023.103856.

19 E. Santos, J. Albo and A. Irabien, Acetate Based Supported Ionic Liquid Membranes (SILMs) for CO2 Separation: Influence of the Temperature, *J. Membr. Sci.*, 2014, **452**, 277–283, DOI: 10.1016/j.memsci.2013.10.024.

20 P. Cserjési, N. Nemestóthy and K. Bélafi-Bakó, Gas Separation Properties of Supported Liquid Membranes Prepared with Unconventional Ionic Liquids, *J. Membr. Sci.*, 2010, **349**(1), 6–11, DOI: 10.1016/j.memsci.2009.10.044.

21 J. E. Bara, T. K. Carlisle, C. J. Gabriel, D. Camper, A. Finotello, D. L. Gin and R. D. Noble, Guide to CO2 Separations in Imidazolium-Based Room-Temperature Ionic Liquids, *Ind. Eng. Chem. Res.*, 2009, **48**(6), 2739–2751, DOI: 10.1021/ie8016237.

22 P. Scovazzo, J. Kieft, D. A. Finan, C. Koval, D. DuBois and R. Noble, Gas Separations Using Non-Hexafluorophosphate [PF6]– Anion Supported Ionic Liquid Membranes, *J. Membr. Sci.*, 2004, **238**(1), 57–63, DOI: 10.1016/j.memsci.2004.02.033.

23 A. J. B. Kemperman, D. Bargeman, Th. Van Den Boomgaard and H. Strathmann, Stability of Supported Liquid Membranes: State of the Art, *Sep. Sci. Technol.*, 1996, **31**(20), 2733–2762, DOI: 10.1080/01496399608000824.

24 I. Kammakakam, J. E. Bara, E. M. Jackson, J. Lertxundi, D. Mecerreyes and L. C. Tomé, Tailored CO2-Philic Anionic Poly(Ionic Liquid) Composite Membranes: Synthesis, Characterization, and Gas Transport Properties, *ACS Sustainable Chem. Eng.*, 2020, **8**(15), 5954–5965, DOI: 10.1021/acssuschemeng.0c00327.

25 E. I. Privalova, E. Karjalainen, M. Nurmi, P. Mäki-Arvela, K. Eränen, H. Tenhu, D. Yu. Murzin and J.-P. Mikkola, Imidazolium-Based Poly(Ionic Liquid)s as New Alternatives for CO2 Capture, *ChemSusChem*, 2013, **6**(8), 1500–1509, DOI: 10.1002/cssc.201300120.

26 Y. Ye and Y. A. Elabd, Anion Exchanged Polymerized Ionic Liquids: High Free Volume Single Ion Conductors, *Polymer*, 2011, **52**(5), 1309–1317, DOI: 10.1016/j.polymer.2011.01.031.

27 J. L. Pablos, N. García, L. Garrido, J. Guzmán, F. Catalina, T. Corrales and P. Tiemblo, Highly Efficient Mixed Li+ Transport in Ion Gel Polycationic Electrolytes, *J. Membr. Sci.*, 2018, **545**, 133–139, DOI: 10.1016/j.memsci.2017.08.073.

28 Y. Li, H. Xiao, Z. Zhang, W. Li, T. Hu, C. Wang and X. Li, UV-crosslinkable imidazolium salt type polymer antibacterial agent and its preparation method, CN102942812, 2013.

29 R. Pulukkody, K. R. Baca, S. N. Lak, A. Butler-Christodoulou, M. B. Shiflett and E. B. Pentzer, Synthesis and Characterization of Fluorinated Ionic Liquids and Their Application in Hydrofluorocarbon Gas Uptake, *Ind. Eng. Chem. Res.*, 2024, **63**(19), 8761–8771, DOI: 10.1021/acs.iecr.4c00370.

30 R. Pulukkody, Y. J. Lee, T. H. Ware and E. B. Pentzer, Mesomorphism of Imidazolium-Based Fluorinated Ionic Liquids, *J. Ionic Liq.*, 2024, 100085, DOI: 10.1016/j.jil.2024.100085.

31 Y. Ye and Y. A. Elabd, Anion Exchanged Polymerized Ionic Liquids: High Free Volume Single Ion Conductors, *Polymer*, 2011, **52**(5), 1309–1317, DOI: 10.1016/j.polymer.2011.01.031.

32 M. G. Cowan, D. L. Gin and R. D. Noble, Poly(Ionic Liquid)/Ionic Liquid Ion-Gels with High "Free" Ionic Liquid Content: Platform Membrane Materials for CO2/Light Gas Separations, *Acc. Chem. Res.*, 2016, **49**(4), 724–732, DOI: 10.1021/acs.accounts.5b00547.

33 I. Kammakakam, K. E. O'Harra, E. M. Jackson and J. E. Bara, Synthesis of Imidazolium-Mediated Poly(Benzoxazole) Ionene and Composites with Ionic Liquids as Advanced Gas Separation Membranes, *Polymer*, 2021, **214**, 123239, DOI: 10.1016/j.polymer.2020.123239.

34 I. Kammakakam, J. E. Bara and E. M. Jackson, Dual Anion–Cation Crosslinked Poly(Ionic Liquid) Composite Membranes for Enhanced CO2 Separation, *ACS Appl. Polym. Mater.*, 2020, **2**(11), 5067–5076, DOI: 10.1021/acsapm.0c00877.

35 A. N. Harders, H. Uhl, I. Xu, S. Dixon, K. R. Baca, T. May, M. D. Lundin and M. B. Shiflett, Ionic Liquid Fluoropolymer Membranes for the Separation of R-410A: Understanding the Effect of Ionic Liquid on Membrane Characteristics and Separation Performance, *J. Membr. Sci.*, 2024, **709**, 123068, DOI: 10.1016/j.memsci.2024.123068.

36 K. Hunger, N. Schmeling, H. B. T. Jeazet, C. Janiak, C. Staudt and K. Kleinermanns, Investigation of Cross-Linked and Additive Containing Polymer Materials for Membranes with Improved Performance in Pervaporation and Gas Separation, *Membranes*, 2012, **2**(4), 727–763, DOI: 10.3390/membranes2040727.

37 L. Chancelier, O. Boyron, T. Gutel and C. Santini, Thermal Stability of Imidazolium-Based Ionic Liquids, *Fr.-Ukr. J. Chem.*, 2016, **4**(1), 51–64, DOI: 10.17721/fujcV4I1P51-64.

38 C. Maton, N. D. Vos and C. V. Stevens, Ionic Liquid Thermal Stabilities: Decomposition Mechanisms and Analysis Tools, *Chem. Soc. Rev.*, 2013, **42**(13), 5963–5977, DOI: 10.1039/C3CS60071H.

39 J. Zhang, F. She, W. Gao and L. Kong, *Preparation of Cross-Linked Nanoporous Poly(Ethylene Glycol) Diacrylate Membrane in Hexagonal Lyotropic Liquid Crystal Phases*, 2009.

40 Z.-X. Low, P. M. Budd, N. B. McKeown and D. A. Patterson, Gas Permeation Properties, Physical Aging, and Its Mitigation in High Free Volume Glassy Polymers, *Chem. Rev.*, 2018, **118**(12), 5871–5911, DOI: 10.1021/acs.chemrev.7b00629.

41 J. E. Bara, E. S. Hatakeyama, D. L. Gin and R. D. Noble, Improving CO2 Permeability in Polymerized Room-Temperature Ionic Liquid Gas Separation Membranes through the Formation of a Solid Composite with a Room-Temperature Ionic Liquid, *Polym. Adv. Technol.*, 2008, **19**(10), 1415–1420, DOI: 10.1002/pat.1209.

42 H. Nulwala, A. Mirjafari and X. Zhou, Ionic Liquids and Poly(Ionic Liquid)s for 3D Printing – A Focused Mini-Review, *Eur. Polym. J.*, 2018, **108**, 390–398, DOI: 10.1016/j.eurpolymj.2018.09.023.

43 C. Pierucci, L. Paleari, J. Baker, C. C. M. Sproncken, M. Folkesson, J. P. Wesseler, A. Vracar, A. Dodero, F. Nanni, J. A. Berrocal, M. Mayer and A. Ianiro, Nafion Membranes for Power Generation from Physiologic Ion Gradients, *RSC Appl. Polym.*, 2025, **3**, 209–221, DOI: 10.1039/D4LP00294F.

44 M. Rist and A. Greiner, Bio-Based Electrospun Polyamide Membrane – Sustainable Multipurpose Filter Membranes for Microplastic Filtration, *RSC Appl. Polym.*, 2024, **2**(4), 642–655, DOI: 10.1039/D3LP00201B.

45 Ľ. Hodásová, I. Isarn, F. Bravo, C. Alemán, N. Borràs, G. Fargas and E. Armelin, Synthesis of Bio-Sourced Liquid Resins and Their Photopolymerization with Poly(Ethylene Glycol) Diacrylate in the Roadmap to More Sustainable Digital Light Processing Technologies, *RSC Appl. Polym.*, 2024, **2**(2), 284–295, DOI: 10.1039/D3LP00207A.

46 F. Klincewicz, S. Kalidindi and L. T. J. Korley, Tuning the Thermal Response of 3D-Printed Bilayer Hydrogels via Architectural Control Using Binary Ethanol–Water Solvent Systems, *RSC Appl. Polym.*, 2024, **2**(6), 1062–1073, DOI: 10.1039/D4LP00032C.

47 B. Narupai, J. Wong, E. Sanchez-Rexach, J. Smith-Jones, V. C. T. Le, N. Sadaba, H. Sardon and A. Nelson, 3D Printing of Ionic Liquid Polymer Networks for Stretchable Conductive Sensors, *Adv. Mater. Technol.*, 2023, **8**(23), 2300226, DOI: **10.1002/admt.202300226**.

48 J. Sun, S. Zhou, Z. Zhao, F. Zhang, Z. Guo, S. Liu and Y. Lu, Facile Fabrication of a Stretchable, Stable, and Self-Adhesive Poly(Ionic Liquid) as a Flexible Sensor, *RSC Appl. Polym.*, 2024, **2**(2), 205–213, DOI: **10.1039/D3LP00137G**.

49 I. Roppolo, M. Zanatta, G. Colucci, R. Scipione, J. M. Cameron, G. N. Newton, V. Sans and A. Chiappone, Digital Light Processing 3D Printing of Polymerizable Ionic Liquids towards Carbon Capture Applications, *React. Funct. Polym.*, 2024, **202**, 105962, DOI: **10.1016/j.reactfunctpolym.2024.105962**.

50 K. R. Hossain, P. Jiang, X. Yao, X. Yang, D. Hu and X. Wang, Ionic Liquids for 3D Printing: Fabrication, Properties, Applications, *J. Ionic Liq.*, 2023, **3**(2), 100066, DOI: **10.1016/j.jil.2023.100066**.

51 M. Gillono, A. Chiappone, L. Mendola, M. Gomez Gomez, L. Scaltrito, C. F. Pirri and I. Roppolo, Study on the Printability through Digital Light Processing Technique of Ionic Liquids for CO2 Capture, *Polymers*, 2019, **11**(12), 1932, DOI: **10.3390/polym11121932**.